Title
Particle sensing with confined optical field enhanced fluorescence emission (Cofefe).

Journal
Optics express, 26(10)

ISSN
1094-4087

Authors
Kenison, John P
Fast, Alexander
Matthews, Brandon M
et al.

Publication Date
2018-05-01

DOI
10.1364/oe.26.012959

Peer reviewed

Research Article | Vol. 26, No. 10 | 14 May 2018 | OPTICS EXPRESS 12959
Optics EXPRESS

Particle sensing with confined optical field enhanced fluorescence emission (Cofefe)

JOHN P. KENISON,[1] ALEXANDER FAST,[2] BRANDON M. MATTHEWS,[2] ROBERT M. CORN,[2] AND ERIC OLAF POTMA[2,*]

[1]*Department of Physics and Astronomy, University of California, Irvine, CA 92697, USA*
[2]*Department of Chemistry, University of California, Irvine, CA 92697, USA*
[*]*epotma@uci.edu*

Abstract: We describe the development and performance of a new type of optical sensor suitable for registering the binding/dissociation of nanoscopic particles near a gold sensing surface. The method shares similarities with surface plasmon resonance microscopy but uses a completely different optical signature for reading out binding events. This new optical read-out mechanism, which we call confined optical field enhanced fluorescence emission (Cofefe), uses pulsed surface plasmon polariton fields at the gold/liquid interface that give rise to confined optical fields upon binding of the target particle to the gold surface. The confined near-fields are sufficient to induce two-photon absorption in the gold sensor surface near the binding site. Subsequent radiative recombination of the electron-hole pairs in the gold produces fluorescence emission, which can be captured by a camera in the far-field. Bound nanoparticles show up as bright confined spots against a dark background on the camera. We show that the Cofefe sensor is capable of detecting gold and silicon nanoparticles, as well as polymer nanospheres and sub-μm lipid droplets in a label-free manner with average illumination powers of less than 10 μW/μm^2.

OCIS codes: (190.4350) Nonlinear optics at surfaces; (240.6680) Surface plasmons; (280.4788) Optical sensing and sensors.

References and links

1. L. M. Zhang, and D. Uttamchandani, "Optical chemical sensing employing surface plasmon resonance," Electron. Lett.**24** (23), 1469–1470 (1988).
2. J. Homola, S. S. Yee, and G. Gauglitz, "Surface plasmon resonance sensors: review," Sensor. Actuat. B-Chem. **54**(1), 3–15 (1999).
3. C. Hahnefeld, S. Drewianka, and F. W. Herberg, "Determination of Kinetic Data Using Surface Plasmon Resonance Biosensors" in *Molecular Diagnosis of Infectious Diseases*, J. Decker, U. Reischl., eds. (Humana Press, 2004), pp 299–320.
4. C. Boozer, G. Kim, S. Cong, H. Guan, and T. Londergan, "Looking towards label-free biomolecular interaction analysis in a high-throughput format: a review of new surface plasmon resonance technololgies," Curr. Opin. Biotech. **17**(4), 400–405 (2006).
5. J. Homola, "Surface plasmon resonance sensor for detection of chemical and biological species," Chem. Rev. **108**, 462–493 (2008).
6. K. S. Phillips, and Q. Cheng, "Recent advances in surface plasmon resonance based techniques for bioanalysis," Anal. Bioanal. Chem. **387**(5), 1831–1840 (2007).
7. P. Singh, "SPR biosensors: historical perspectives and current challenges," Sens. Actuators B-Chem. **229**, 110–130 (2016).
8. C. E. Jordan, A.G. Frutos, A. J. Thiel, and R. M. Corn, "Surface plasmon resonance imaging measurements of DNA hybridization adsorption and streptavadin/DNA multilayer formation at chemically modified gold surfaces," Anal. Chem. **69**(24), 4939–4947 (1997).
9. J. M. Brockman, B. P. Nelson, and R. M. Corn, "Surface plasmon resonance imaging measurements of ultrathin organic films," Annu. Rev. Phys. Chem. **51**, 41–63 (2000).
10. H. Kano and W. Knoll, "A scanning microscope employing localized surface-plasmon-polaritons as a sensing probe," Opt. Commun. **182**(1), 11–15 (2000).
11. B. Huang, F. Yu, and R. N. Zare, "Surface plasmon resonance imaging using a high numerical aperture microscope objective," Anal. Chem. **79**(7), 2979–2983, (2007).
12. F. Weichert, M. Gaspar, C. Timm, A. Zybin, E. L. Gurevich, M. Engel, H. Müller, and P. Marwedel, "Signal analysis and classification fir surface plasmon assisted microscopy of nanoobjects," Sens. Actuators B-Chem. **151**(1), 281–290

#323176 https://doi.org/10.1364/OE.26.012959
Journal © 2018 Received 15 Feb 2018; revised 5 Apr 2018; accepted 23 Apr 2018; published 4 May 2018

Optics EXPRESS

(2010).
13. W. Wang, Y. Yang, S. Wang, V. J. Nagaraj, Q. Liu, J. Wu, and N. Tao, "Label-free measuring and mapping of binding kinetics of membrane proteins in single living cells," Nat. Chem. **4**(10), 846–853 (2012).
14. K. Syal, R. Iriya, Y. Yang, H. Yu, S. Wang, S. E. Haydel, H. Y. Chen, and N. Tao, "Antimicrobial susceptibility test with plasmonic imaging and tracking of single bacterial motions on nanometer scale," ACS Nano **10**(1), 845–852 (2016).
15. S. Wang, X. Shan, U. Patel, X. Huang, J. Lu, J. Li, and N. Tao, "Label free imaging, detection, and mass measurement of single viruses by surface plasmon resonance," Proc. Natl. Acad. Sci. **107**(37), 16028–16032 (2010).
16. H. Yu, X. Shan, S. Wang, H. Chen, and N. Tao, "Plasmonic imaging and detection of single DNA molecules," ACS Nano **8**(4), 3427–3433 (2014).
17. A. R. Halpern, J. B. Wood, Y. Wang, and R. M. Corn, "Single-nanoparticle near-infrared surface plasmon resonance microscopy for real-time measurements of of DNA hybridization adsorption," ACS Nano **8**(1), 1022–1030 (2014).
18. A. M Maley, G.J. Lu, M.G. Shapiro, and R. M. Corn, "Characterizing single polymeric and protein nanoparticles with surface plasmon resonance imaging measurements," ACS Nano **11**(7), 7447–7456 (2017).
19. H. Raether, "Surface plasma oscillations and their applications," in *Physics of Thin Films*, G. Hass, M. Francombe, and R. Hoffman, eds. (Academic, 1977).
20. R. P. H. Kooyman, H. Kolkman, J. Van Gent, and J. Greve, "Surface plasmon resonance immunosensors: sensitivity considerations," Anal. Chim. Acta **213** (Supplement C), 35–45, (1988).
21. H. Yu, X. Shan, S. Wang, and N. Tao, "Achieving high spatial resolution surface plasmon resonance microscopy with image reconstruction," Anal. Chem. **89**(5), 2704–2707, (2017).
22. I. Gryczynski, J. Malicka, J.R. Lakowicz, E.M. Goldys, N. Calander, and Z. Gryczynski, "Directional two-photon induced surface plasmon-coupled emission," Thin Solid Films **491**(1), 173–176 (2005).
23. R. He, Y. Su, K. Cho, C. Lin, N. Chang, C. Chang, and S. Chen, "Surface plasmon-enhanced two-photon fluorescence microscopy for live cell membrane imaging," Opt. Express **17**(8), 5987–5997 (2009).
24. A. Mooradian, "Photoluminescence of metals," Phys. Rev. Lett. **22**(5), 185 (1969).
25. G. T. Boyd, Z. H. Lu, and Y. R. Shen, "Photoinduced luminescence from the noblemetals and its enhancement on roughened surfaces," Phys. Rev. B **33**(33), 7923–7936 (1986).
26. M. R Beversluis, A. Bouhelier, and L. Novotny, "Continuum generation from single gold nanostructures through near-field mediated intraband transitions," Phys. Rev. B **68**(11), 115433 (2003).
27. A. G. Cullis and L. T. Canham, "Visible light emission due to quantum size effects in highly porous crystalline silicon," Nature **353**, 335–338 (1991).
28. W. L. Wilson, P. F. Szajowski, and L. E. Brus, "Quantum confinement in size-selected, surface-oxidized silicon nanocrystals," Science **262**, 1242–1244 (1993).
29. B. Dubertret, P. Skourides, D. J. Norris, V. Noireaux, A. H. Brivanlou, and A. Libchaber, 1759–1762, "In vivo imaging of quantum dots encapsulated in phospholipid micelles," Science **298** (2002).
30. K. I. Mortensen, L. S. Churchman, J. A. Spudich, and H. Flyvbjerg, "Optimized localization analysis for single-molecule tracking and super-resolution microscopy," Nat. Meth **7(5)**, 377–381 (2010).
31. L. Schermelleh, R. Heintzmann, and H. Leonhardt, "A guide to super-resolution fluorescence microscopy," J. Cell. Biol. **190**(2), 165–175 (2010).
32. N. Gustafsson, S. Culley, G. Ashdown, D. M. Owen, P. M. Pereira, and R. Henriques, "Fast live-cell conventional fluorophore nanoscopy with ImageJ through super-resolution radial fluctuations," Nat. Comm. **7**, 12471 (2016).
33. J. P. Kenison, A. Fast, F. Guo, A. LeBon, W. Jiang, and E. O. Potma, "Imaging properties of surface-enhanced coherent anti-Stokes Raman scattering microscopy on thin gold films," J. Opt. Soc. Am. B **34**(10), 2104–2114 (2017).
34. J. R. Lakowicz, J. Malicka, I. Gryczynski, and Z. Gryczynski, "Directional surface plasmon-coupled emission: a new method for high sensitivity detection," Biochem. Bioph. Res. Co. **307**(3), 435–439 (2003).
35. I. Gryczynski, J. Malicka, Z. Gryczynski, and J. R. Lakowicz, "Surface plasmon-coupled emission with gold films," J. Phys. Chem. B **108**(33), 12568–12574 (2004).
36. F. D. Stefani, K. Vasilev, N. Bocchio, N. Stoyanova, and M. Kreiter, "Surface-plasmon-mediated single-molecule fluorescence through a thin metallic film," Phys. Rev. Lett. **94**(2), 023005 (2005).
37. J. Borejdo, N. Calander, Z. Gryczynski, and I. Gryczynski, "Fluorescence correlation spectroscopy in surface plasmon coupled emission microscope," Opt. Express **14**(17), 7878–7888 (2006).
38. C. Lin, K. Chiu, C. Chang, S. Chang, T. Guo, and S. Chen, "Surface plasmon-enhanced and quenched two-photon excited fluorescence," Opt. Express **18**(12), 12807–12817 (2010).
39. S. Cao, W. Cai, Q. Liu, and Y. Li, "Surface plasmon-coupled emission: what can directional fluorescence bring to the analytical sciences?," Annu. Rev. Phys. Chem. **5**, 317–336 (2012).
40. S. H. Cao, W. P. Cai, Q. Liu, K. X. Xie, Y. H. Weng, S.-X. Huo, Z.-Q. Tian, and Y.-Q. Li, "Label-free aptasensor based on ultrathin-linker-mediated hot-spot assembly to induce strong directional fluorescence," J. Am. Chem. Soc. **136**(19), 6802–6805 (2014).
41. S.-H. Cao, Y.-Y. Zhai, K.-X. Xie, and Y.-Q. Li, "Surface Plasmon-Coupled Emission," in *Surface Plasmon Enhanced, Coupled and Controlled Fluorescence*, C. D. Geddes, ed. (John Wiley & Sons, 2017).
42. W. T. Tang, E. Chung, Y.-H. Kim, P. T. C. So, and C. J. R. Sheppard, "Investigation of the point spread function of surface plasmon-coupled emission microscopy," Opt. Express **15**(8), 4634–4646 (2007).
43. W. T. Tang, E. Chung, Y.-H. Kim, P. T. C. So, and C. J. R. Sheppard, "Surface-plasmon-coupled emission microscopy

Optics EXPRESS

with a spiral phase plate," Opt. Lett. **35**(4), 517–519 (2010).
44. B. Ge, Y. Ma, C. Kuang, D. Zhang, K. C. Toussaint, Jr, S. You, and X. Liu, "Resolution-enhanced surface plasmon-coupled emission microscopy," Opt. Express **23**(10), 13159–13171 (2015).

1. Introduction

Surface plasmon resonance (SPR) sensing is a technology used for measuring binding and dissociation kinetics of biomolecules at a gold sensor surface. [1–7] Such biomolecular interactions include interactions among proteins, peptides, nucleotides, sugars and other molecules. In pharmaceutical, clinical and biotechnological research, for instance, knowledge of biomolecular interactions is key in determining efficacy of a drug, understanding immunological responses or discovering new therapeutic targets, to name just a few.

Whereas the SPR technique is very sensitive, its common implementation is unable to detect individual binding and dissociation events. Kinetic SPR data is typically the result of ensemble averaging over many events, integrated over both space and time. Consequently, rapid on/off events at particular sites on the sensor surface are not registered, as they are averaged out by the slower dynamics of the ensemble. Other unexpected binding patterns at particular sites also go unnoticed. Such outlier behavior can be important, as these events may signify functional aspects of the molecular interaction, related to particular conformations, density related binding kinetics or other effects of direct relevance. The ability to see all binding/dissociation events in parallel would significantly enhance the analytical capabilities of the SPR sensor.

Individual binding/dissociation events can be studied with a microscopic imaging version of SPR, namely surface plasmon resonance microscopy (SPRM). [8–12] The latter technique makes it possible to visualize individual events in parallel with a camera, thus enabling multiplex detection of particles interacting at the sensor surface. SPRM has been successfully employed to probe individual cells [13], bacteria and viruses [14,15], DNA [16,17], and protein structures. [18] The ultimate sensitivity of SPRM is limited by various factors. [19–21] One limitation is related to the fact that SPR methods are not background-free, as small changes in the light intensity need to be discriminated against a bright background. Another limiting factor is the non-ideal pointspread function of SPRM, which is characterized by long diffractive tails that affect the spatial resolution of the technique. To increase the spatial resolution, special algorithms have been developed that improve the performance of the SPRM device, achieving an effective resolution on the sub-micrometer scale. [21] Nonetheless, the restored pointspread function is non-symmetric and may exhibit residual flaring.

The SPRM technology would benefit from an optical signaling mechanism that is associated with a well-behaved pointspread function and that produces a positive signal relative to a low background. In this work, we present an optical signature at the gold sensor surface that overcomes the aforementioned issues. The signal, which we attribute to two-photon excited fluorescence in the gold film, is triggered by binding of particles to the surface. The pointspread function, which appears against a dark background, is incoherent and thus devoid of interferences among detected spots. The resulting technique is related to two-photon surface plasmon-coupled emission (SPCE) microscopy [22,23], but without the need to incorporate fluorophores and thus allowing label-free probing of targets. We discuss the optical layout of this new approach and present its capabilities for detecting individual particles in the vicinity of the sensor surface.

2. Materials and methods

2.1. Microscope setup

A schematic of the sensor device is shown in Fig. 1. The light source is a Titanium:sapphire laser (Mira900, Coherent), which produces a 76 MHz pulse train of ~200 fs pulses. In the experiments the center wavelength is set to 800 nm. The linearly polarized source is conditioned with a spatial

Optics EXPRESS

filter to generate a clean Gaussian transverse profile of 10 mm diameter. The collimated beam is then focused by a f = 250 mm lens onto the back focal plane of a high numerical aperture objective (NA 1.49 oil, Olympus). The resulting collimated beam emerging from the objective corresponds to a circular illumination spot with a diameter of ~ 120 μm on the sensor surface. The sensor surface consists of a borosilicate coverslip coated with a 30 nm thick gold film. By translating the beam in the back focal plane, the incidence angle of the collimated beam at the surface can be tuned to the Kretschmann angle for excitation of a surface plasmon polariton (SPP) mode at the gold/water interface (~ 65^o). The resulting two-photon luminescence from the gold film is collected in the epi-direction by the objective and separated from the incident beam by a 700 nm short wave pass dichroic mirror. The signal is subsequently filtered by a 625 nm±45 nm band pass filter and 750 nm short wave pass filter. In some of the experiments, a 1.6× telescope is incorporated in the detection path for increased magnification, resulting in an image distance of 169.5 nm per pixel with a ~ 60 μm diameter field of view (FOV). Average illumination powers, determined before the objective lens, are between 15 mW and 70 mW, depending on the FOV and the sample. For each of the experiments that follow, the illumination dose is specified in $\mu W/\mu m^2$, which is independent of the FOV. Note that the actual dose at the sample is lower because of losses in the objective lens and specimen. The signal is recorded on an EM-CCD camera (iXon3, Andor) as stacks of images (512 × 512 pixels) with a frame rate of 1 fps. Higher acquisition rates may be obtained with a reduced region of interest (ROI). For instance, for a ROI of 256 × 256 pixels, the signal can be recorded at 68 fps.

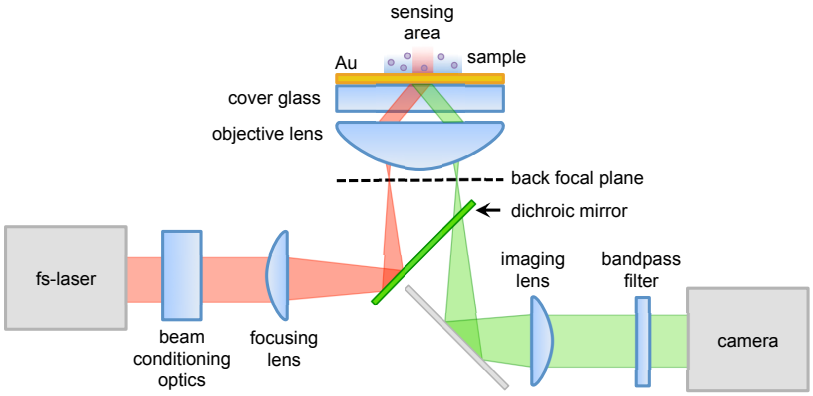

Fig. 1. Schematic of the sensor device. A fs-laser beam is focused on the back focal plane of a high NA objective lens, launching an SPP field at the sensor surface. Particle binding gives rise to local two-photon excited fluorescence in the gold film, which is captured by an imaging camera.

2.2. Sample preparation

Sensor surfaces consist of borosilicate glass coverslips (BK-7, VWR) coated with gold. Gold thin films are evaporated to a thickness of 30 nm on the coverslips, which are pretreated with a 2 nm Cr adhesion layer. Analytes used in this experiment included gold spheres (10 nm, 20 nm, 30 nm), cholesteryl oleate droplets (Sigma Aldrich), polystyrene spheres (50 nm from Thermo Fisher; 100 nm from PolySciences), and silicon nanoparticles (30 nm, Melorium Technologies). All particle suspensions are diluted in milli-Q filtered water and sonicated before use. Lipid droplets are formed by preparing an emulsion of cholesteryl oleate with phosphatidylcholine in phosphate-buffered saline (PBS). Using ~ 50 μL of a stock solution, the emulsion is subsequently drop cast on the Au-covered microscope coverslips, resulting in air-dried droplets and micrometer-sized polymorphous crystals of cholesteryl oleate on the surface. The structures were re-immersed in

Optics EXPRESS

milli-Q filtered water before inspection with the imaging sensor. Si particles, gold spheres, and PS spheres were all diluted with deionized water and drop cast onto gold-coated coverslips.

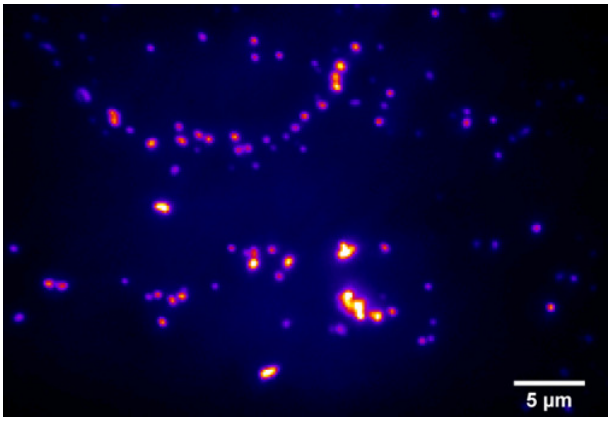

Fig. 2. Gold nanospheres (20nm) adhered to the sensor surface in an aqueous medium. Average power of the illuminating beam before the objective lens is 15 mW.

3. Results

3.1. Detection of gold nanoparticles

We first examine the signal from a bare gold film on glass, using milli-Q filtered water as the sample. For smooth, freshly prepared films, the background signal is near or at the dark count rate of the camera, approximately 100 counts/s. This latter observation indicates that the signal from the bare gold film is very small. However, for older sensor surfaces and at higher illumination doses (up to 28 μW/μm^2), the signal from the bare sensor can reach 370 counts/s.

When gold nanoparticles are deposited on the sensor surface, bright spots are detected that are well above the background. A representative result is depicted in Fig. 2, which shows the detected image on the camera after 20 nm gold particles physisorbed to the sensor surface from solution. Clusters and individual particles can be recognized in the image. The image is only visible when the incident beam is coupled to the gold film at the Kretschmann angle. Small detuning away from the coupling angle results in the disappearance of the signal. Signal is only observed when particles are adhered to the surface, particles suspended in the bulk remain invisible. We observe similar results for gold nanospheres of diameters of 10 and 30 nm.

In Fig. 2, the signal is accumulated over 100 raw frames taken at 68 fps by using a 256×256 ROI of the camera chip (60 μm diameter on the sensor surface) with a 15 mW beam incident on back aperture of the objective lens, corresponding to 5.3 μW/μm^2 average power or less than 78 nJ/μm^2 average energy for each raw frame. Signals clearly distinguishable from the background are still observed when the illumination power is lowered. For instance, at 68 fps, average illumination powers of 5–10 mW (1.8–3.5 μW/μm^2) produce images with detected spots well above the background counts in each frame. When the electron-multiplying (EM) gain is used, with a gain between 25 and 300, illumination powers can be lowered to 1–2 mW (0.36–0.71 μW/μm^2) at the same acquisition speed.

Gold nanoparticles, which are commonly used in SPRM experiments as contrast enhancers, support localized surface plasmons. The enhanced fields associated with the surface plasmon mode can give rise to two-photon excitation of electron-hole pairs in the gold particle, followed by fluorescence emission upon electron-hole recombination. [24–26] Whenever a gold nanoparticle lands on the sensor surface, the local fields are even more enhanced by the nanocavity formed between the particle and the gold layer. It is, therefore, perhaps not surprising that strong

Optics EXPRESS

fluorescent signals from the location of the particles are observed. The results shown in Fig. 2 demonstrate that the nanocavities between the analyte (particle) and the gold film are efficiently excited by the SPP modes on the sensor surface, and that the resulting incoherent emission is conveniently detected by the far-field camera. Next, we examine whether similar results can be obtained for particles that do not support localized surface plasmon modes themselves.

3.2. Detection of semi-conducting nanoparticles

We use 30 nm silicon nanoparticles as non-metallic particles for examining the sensitivity of the sensor to nanoparticles that do not support localized surface plasmon modes. As a consequence, we expect signals that are weaker compared to the case of Au nanoparticles. Figure 3 shows an image of Si nanoparticles physisorbed to the gold surface in an aqueous suspension. At power levels of 4.4 μW/μm^2, the particles are clearly seen. Panel 3(b) shows the logarithm of the fluorescence signal in the indicated region of interest, showing well resolved spots derived from clusters and individual particles. Panel 3(c) depicts the corresponding transmission image, obtained by illuminating the sample with a halogen lamp and detecting the image plane with the same camera. Comparison between the transmission and fluorescence image reveals that whereas the brighter clusters can be seen in the transmission image, the fluorescence image identifies structures that remain invisible in transmission contrast (see encircled area). The latter emphasizes that the sensor can sense structures that cannot be seen through their refractive properties as observed in transmission. Although smaller (< 10 nm) silicon nanoparticles and porous silicon are known to exhibit strong luminescent properties of their own [27–29], the fluorescence from 30 nm sized Si nanoparticles is rather weak. Indeed, we did not observe any fluorescence from the Si particles when dispersed on plain glass coverslips in total internal reflection fluorescence mode under similar excitation conditions, underlining that the signal is only observed when the gold film is present. We note that the fluorescence signal is stable and does not show blinking effects characteristic of semi-conducting quantum dots.

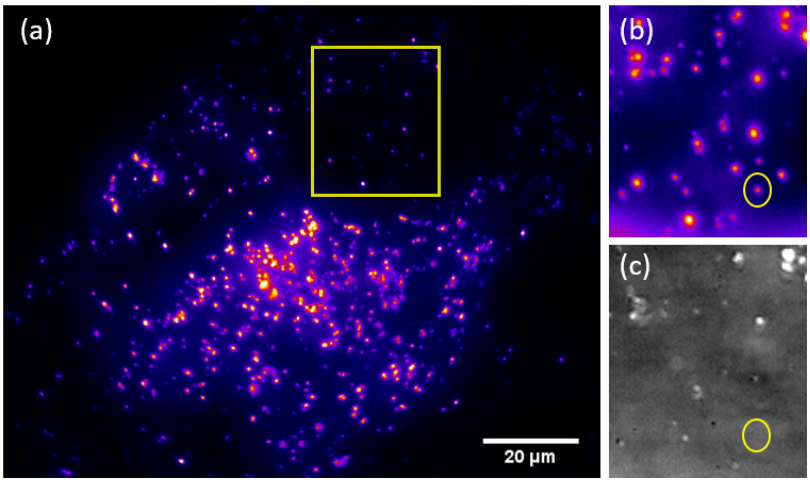

Fig. 3. (a) Sensor image of 30 nm Si nanoparticles in water under illumination of 4.4μW/μm^2. (b) Zoom of the region of interest indicated in (a). The logarithm of the signal is taken to reveal weaker emitters. (c) Transmission image of the same region of interest as in (b).

3.3. Detection of polymer particles and organic matter

Gold and silicon nanoparticles have relatively high dielectric constants, translating in strong refractive properties even when suspended in water. It is more challenging to detect objects with

Optics EXPRESS

a refractive index closer to that of water. We utilize polystyrene beads (100 nm) as an example of a non-fluorescent particle with a relatively low refractive index ($n \approx 1.60$). Figure 4(a) shows a two-photon excited fluorescence image of polystyrene beads adhered to the sensor surface obtained when using $5.2\mu W/\mu m^2$ of average illumination power before the objective. We perform similar measurements with cholesteryl oleate droplets in an aqueous medium, shown in Fig. 4(b). Again, bright fluorescence signals are observed against a low background. Some spots, such as the one indicated by the arrow, have diameters that are sub-μm, indicating that the lipid droplets that trigger the signal are also sub-μm in size. The magnitude of the signal is comparable to the signal obtained from the silicon nano-particles at the sensor surface.

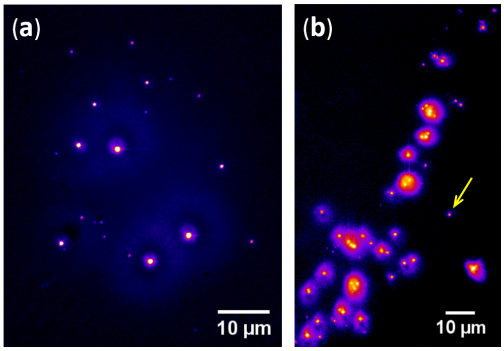

Fig. 4. (a) Polystyrene beads (100 nm) suspended in water. (b) Cholesteryl oleate droplets adhered to the sensor surface. Arrow points to a smaller, sub-μm droplet. In both images, $5.2\mu W/\mu m^2$ of illumination power is used.

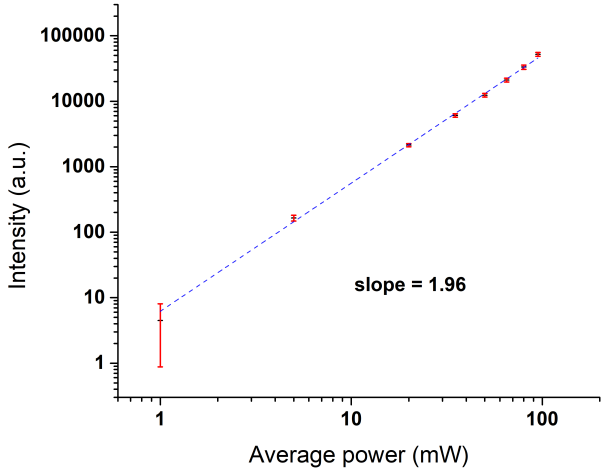

Fig. 5. Magnitude of the fluorescence signal obtained from the locations of cholesteryl oleate droplets as the average power of the illuminating beam is increased. Power is measured at the back aperture of the objective lens.

Figure 5 shows the dependence of the signal generated at the locations of the cholesteryl oleate droplets as the illumination power is increased. We find a power dependence close to 2,

Optics EXPRESS

suggesting that the process responsible for the signal is indeed a two-photon excited fluorescence process. Since both polystyrene and cholesteryl oleate are non-fluorescent, the origin of the signal is not likely the particles themselves. Rather, the experiments suggest that two-photon excited fluorescence originates from the gold sensor surface itself.

3.4. Pointspread function

To obtain a better picture of the imaging properties of the sensor, we perform measurements on 50 nm polystyrene beads. To avoid the probability of cluster formation, we dilute the suspension to such an extent that fewer than 1 detected spot per 10×10 μm^2 is observed on the sensor. Spots are identified by thresholding the image to 0.4 times the standard deviation above the signal distribution of the background. The background distribution collected from a bare sensor surface is subtracted from the data. The resulting distribution of counts obtained from numerous identified spots is shown in 6(a). The distribution exhibits clearly separated peaks. The peak with the lowest number of counts is the most prominent, followed by smaller peaks registered at higher number of counts. The distributions are outlined by Gaussian fits to highlight the features in the histogram. The data suggests that the distribution with the lowest number of counts corresponds to the detection of individual 50 nm particles, with the second peaked distribution resulting from clusters of two particles and so forth.

Figure 6(b) depicts a cross section of an averaged detection spot, obtained by averaging over ten different detected spots that belong to the distribution with the lowest number of counts. The Gaussian fit reveals a full width half maximum (FWHM) of 0.367 μm, which constitutes a measure of the pointspread function (PSF) of the sensor system. The FWHM is virtually invariant among the detected spots. Even the brightest spots ($> 6,000$ counts) exhibit a profile of similar width, indicating that the size of the clusters formed are still below the diffraction limit. Overall, these measurements suggest that the sensor is sensitive enough for detecting individual 50 nm particles with a high signal-to-noise ratio (SNR). In the range between 200 and 2100 counts, the average SNR amounts to 11. Note that the well behaved PSF is suitable for use with super-resolution localization microscopy algorithms. [30–32]

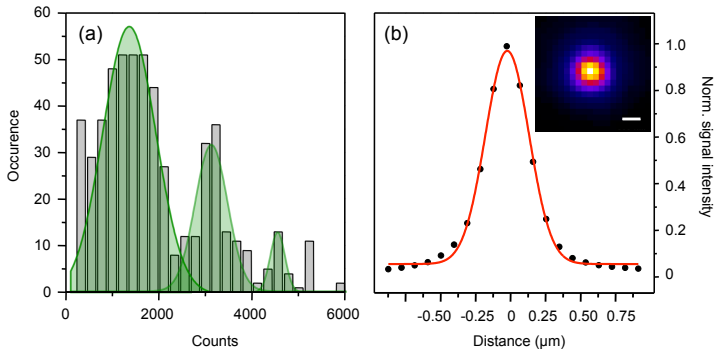

Fig. 6. Analysis of detected signal from 50 nm polystyrene beads. (a) Probability distribution of the number of counts detected in individual isolated spots. The green overlays are Gaussian fits to the first three peaks observed in the histogram to highlight its main features. (b) Cross section of a spot (solid dots), averaged over 10 different detected spots. The red line is a Gaussian fit revealing a width of 0.367 μm. Inset shows the averaged pointspread function. The scale bar is 300 nm.

4. Discussion

In this work, we have constructed a sensor based on the excitation of SPP modes in a thin gold film by a femtosecond laser beam. When the radiation from the film is projected onto a camera, we

Optics EXPRESS

observe clear signals from locations where particles are in close proximity to the gold film. This radiation appears in the spectral window where we expect the two-photon excited fluorescence from gold to be prominent. The experiments described above demonstrate that this signal does not only appear for plasmonically active gold nanoparticles, but also for silicon nanoparticles, polymer beads and sub-μm lipid droplets. These observations strongly suggest that the gold layer itself contributes to the detected radiation. In case of non-fluorescent particles such as polystyrene nanospheres and lipid droplets, the gold layer is expected to be the sole origin of two-photon excited fluorescence.

It is well known that electron-hole pairs can be excited by the process of two-photon absorption in gold. [25, 26] Using a near-infrared laser, electrons are excited from the d-band to the sp-band conduction band, see Fig. 7(a). Radiative electron-hole recombination is expected around symmetry points in the Brillouin zone where the density of states in the conduction band is high. Such a condition is found near the Fermi level of the X and L symmetry points, which correspond to radiative energies of 1.8 eV and 2.4 eV, respectively, upon recombination of momentum-matched electrons in the conduction band and holes in the valence band. In case of confined and enhanced local fields near the gold surface, both the absorption and emission rates are expected to increase, producing efficient two-photon excited fluorescence from gold. [25, 26] The formation of nano-cavities can furthermore relax the photon-momenta, enabling transitions in a broader region near the X and L symmetry points and resulting in a spectrally broadened emission.

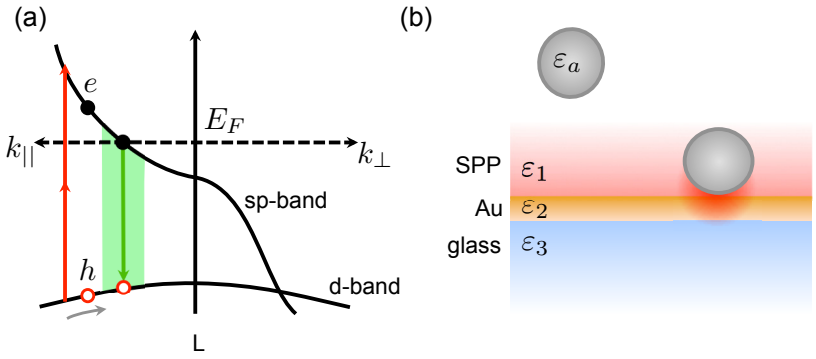

Fig. 7. (a) Band structure of gold and the proposed electron-hole pair generation induced by two-photon absorption (red arrows), followed by radiative recombination (green shaded area). Dashed line denotes the Fermi level. (b) Proposed mechanism of the sensor. A particle of dielectric constant ε_a moves in an aqueous solution of dielectric constant ε_1. Upon illumination through the glass medium (ε_3), SPP modes are excited at the gold/liquid interface. Adsorption of the particle to the gold surface produces confined fields near the binding site, inducing two-photon absorption in the gold layer. Radiative electron-hole recombination is facilitated by the field confinement and the antenna properties of the gold film.

Our results confirm that the two-photon excited fluorescence of the *bare* smooth gold is very inefficient. [26] Under SPP illumination conditions, the gold film itself produces a negligible amount of emission which is near the noise floor of our camera. However, whenever a nanoparticle is in the vicinity of the film, fluorescence emission is observed. This observation suggests that the confinement of the field between the gold and the particle yields local fields sufficient for two-photon excitation of electron-hole pairs in the gold, as schematically depicted in Fig. 7(b). This process is evidently efficient if the nanoparticle is gold, giving rise to strongly enhanced fields, but our experiments show that polymer particles or lipid droplets yield confined fields that are also capable of triggering two-photon absorption.

Optics EXPRESS

The subsequent emission process is furthermore enhanced by the gold film. The emission pattern observed in the back focal plane shows that the majority of the radiation couples out at the Kretschmann angle, indicating that the local polarization near the particle excites surface plasmon polaritons in the film, which subsequently couple to the far field as leakage radiation. [22, 33] This latter mechanism is similar to the enhanced emission seen in SPCE microscopy. [23, 34–39] Previous work in SPCE microscopy has shown the utility of confined local fields to boost the optical signal generated at the gold/sample interface. [40, 41] Our work extends some of the principles developed for SPCE microscopy to include signal generation in the absence of fluorophores, thus constituting a completely label-free approach. In our sensor, the gold film plays a dual role: it is the site of the optical excitation and it acts as an antenna to couple the local polarization in the form of radiation to the far-field.

The mechanism described above is consistent with our observations. We will call this mechanism confined optical field enhanced fluorescence emission, or Cofefe. The Cofefe sensor enables detection of non-fluorescent particles that physisorb to the gold sensor surface. In its current version, the sensor largely reproduces the capabilities of SPRM. However, the detected signal in Cofefe appears relative to a dark background and the detected spot exhibits a pointspread function that is based on incoherent emission and thus does not display interferences among different detected spots. These attributes make the sensor a very attractive alternative to existing SPRM methods.

It is known that the pointspread function in SPCE microscopy is diffraction-limited but, unlike the familiar Airy disk pattern observed in standard fluorescence microscopy, it displays a dip in the center lobe. [42] This feature is due to the antenna-directed fluorescence emission, producing radially polarized radiation as seen at the back aperture of the objective lens. It has been shown that waveplates [43] or differential imaging techniques [44] can be used to restore the PSF to a single-lobed profile. In our measurements, we have observed ring-like PSFs for the gold nanoparticle samples, indicating that the SPCE mechanism is at play. However, for non-fluorescent particles we do not clearly observe donut-shaped profiles but rather single-lobed PSFs, such as shown in Fig. 6(b) for 50 nm polystyrene spheres. This observation suggests that the imaging theory developed for a fluorophore placed in the space above the gold film may not fully capture the properties of the Cofefe sensor. In this context we note that the electron-hole pair generation and recombination responsible for the radiation takes place in the gold layer rather than in the aqueous medium above the sensor surface, and thus represents a different situation than in SPCE. Future work will focus on developing an imaging theory that properly describes the signal radiation process relevant to Cofefe.

The experiments described here are based on simple physisorption of particles to the gold surface. By functionalizing the gold surface it is relatively straightforward to turn the Cofefe sensor into a device for specific binding and sensing studies. The Cofefe signals are strong, enabling detection of organic material such as small lipid droplets at high frame rates in a label-free manner. Our results point to the possibility of detecting much smaller particles, such as liposomes, low-density lipoprotein (LDL) particles or viruses. In addition, the performance of the device can be improved, for instance by optimizing the pulse parameters, detection filters and quality of the gold sensing surface. We expect that the sensor may eventually be sensitive enough for detecting signals from individual protein structures. Such a capability would represent a significant advance in the label-free analysis of protein-ligand interactions on a single molecule level.

5. Conclusion

We have constructed a sensor that enables the detection of particles near a gold sensing surface. The optical signal is based on the two-photon excited fluorescence from the gold, enabled by the formation of confined optical fields upon binding/adsorption of the particle to the substrate. We

Optics EXPRESS

have shown that this sensor, called Cofefe, is capable of registering non-fluorescent particles through the process of gold fluorescence. Unlike SPR-based sensors, the Cofefe method produces background-free signals and yields non-interfering and highly confined spots on the camera detector. These attributes make the Cofefe sensor an attractive candidate for label-free binding and sensing studies, tentatively on the single protein level.

Funding

National Science Foundation (DBI-1454885, CHE-1414466); National Institutes of Health (R01-GM059622).

Acknowledgments

We thank Alexander LeBon for assisting in early editions of the experiments.